A model for influence of exercise on formation and growth of tissue bubbles during altitude decompression

Philip P. Foster, Alan H. Feiveson, Roland Glowinski, Michael Izygon and Aladin M. Boriek

Am J Physiol Regulatory Integrative Comp Physiol 279:2304-2316, 2000.

Am J Physiol Regulatory Integrative Comp Physiol
279: R2304–R2316, 2000.

A model for influence of exercise on formation and growth of tissue bubbles during altitude decompression

PHILIP P. FOSTER,[1] ALAN H. FEIVESON,[2] ROLAND GLOWINSKI,[3]
MICHAEL IZYGON,[4] AND ALADIN M. BORIEK[1]
[1]*Department of Medicine, Baylor College of Medicine, Houston 77030;* [2]*Medical Sciences Division, National Aeronautics and Space Administration Johnson Space Center, Houston 77058; and* [3]*Division of Mathematics and* [4]*Department of Physics, University of Houston, Houston, Texas 77004*

Received 20 April 2000; accepted in final form 3 August 2000

Foster, Philip P., Alan H. Feiveson, Roland Glowinski, Michael Izygon, and Aladin M. Boriek. A model for influence of exercise on formation and growth of tissue bubbles during altitude decompression. *Am J Physiol Regulatory Integrative Comp Physiol* 279: R2304–R2316, 2000.—In response to exercise performed before or after altitude decompression, physiological changes are suspected to affect the formation and growth of decompression bubbles. We hypothesized that the work to change the size of a bubble is done by gas pressure gradients in a macro- and microsystem of thermodynamic forces and that the number of bubbles formed through time follows a Poisson process. We modeled the influence of tissue O_2 consumption on bubble dynamics in the O_2 transport system in series against resistances, from the alveolus to the microsystem containing the bubble and its surrounding tissue shell. Realistic simulations of experimental decompression procedures typical of actual extravehicular activities were obtained. Results suggest that exercise-induced elevation of O_2 consumption at altitude leads to bubble persistence in tissues. At the same time, exercise-enhanced perfusion leads to an overall suppression of bubble growth. The total volume of bubbles would be reduced unless increased tissue motion simultaneously raises the rate of bubble formation through cavitation processes, thus maintaining or increasing total bubble volume, despite the exercise.

macro- and microsystem; O_2 serial transport; O_2 tissue uptake; O_2 window; N_2 supersaturation; Poisson process

ASTRONAUTS PERFORMING EXTRAVEHICULAR activities (EVAs), when exposed to a reduced absolute pressure in their space suits, may experience decompression illness (DCI) (6–8). The primary cause of DCI is the formation and growth of gas bubbles within tissues evolving from excess dissolved gases (7, 8). It has been suggested that metabolic gases make up significant fractions of the gas in bubbles during altitude decompression (11, 41). In tissues supersaturated with an inert gas, typically N_2, in the presence of O_2 (30, 45), CO_2, and water vapor, de novo bubbles are generated from primordial gaseous entities, "gas micronuclei." The initial explosive bubble growth involves the surrounding tissue (11, 40) and may recruit all dissolved gases. To reduce bubble formation and growth, a denitrogenation or N_2 "washout" procedure consisting of prebreathing a hyperoxic mixture is performed before ascent to a constant working altitude pressure. We refer to the overall sequence of O_2 prebreathe, ascent, and time at altitude as a "decompression profile." When referring to the actual process of pressure reduction, however, we use the simpler term "decompression." Bubbles may form, grow, and decay during the sojourn at altitude, usually disappearing on recompression to sea level.

It has become increasingly apparent that skeletal muscle exercise, regardless of when it is performed, influences the onset of DCI (20, 48). A possible explanation is that exercise may create gas micronuclei (44). In particular, high-intensity exercise before decompression may create gas micronuclei (19), which increase the risk of DCI. Also, mechanical movement of body structures may cause cavitation (19) and increase the production of bubbles after decompression (20). Although exercise may accelerate N_2 elimination, it does not invariably precipitate bubble formation (20) and, therefore, may even induce a protection against DCI. Experimental results from Webb et al. (48) indicated that moderate exercise performed during the O_2-prebreathe period enhanced the tissue N_2 washout and reduced the incidence of DCI. Here, we develop a bubble formation-and-growth model (FGM) to answer the following questions. First, how do exercise-induced mechanisms impact formation and growth of gas bubbles? Second, are these mechanisms competing, and if so how? In the accompanying study (11a), the FGM will be validated in a survival analysis to predict the incidence of DCI in the National Aeronautics and Space Administration Altitude Experimental Data Set.

A bubble is defined as a volume of gas in a tissue that follows the phenomenological laws of ideal gases, diffusion and surface tension (40). Bubble growth is controlled by the classical laws of motion: the pressure of the gas provides the driving force to expand the bubble, while the inertia and elastic recoil of the tissue, to-

Address for reprint requests and other correspondence: P. P. Foster, Pulmonary and Critical Care Section, Dept. of Medicine, Baylor College of Medicine, 6550 Fannin St., Smith Tower, Suite 1225, Houston, TX 77030 (E-mail: philipf@bcm.tmc.edu).

The costs of publication of this article were defrayed in part by the payment of page charges. The article must therefore be hereby marked "*advertisement*" in accordance with 18 U.S.C. Section 1734 solely to indicate this fact.

gether with the interfacial tension of the bubble wall, provide resistance to expansion (40). The actual work to change the bubble volume is accomplished solely by pressure gradients of gases across the interface between the bubble and surrounding tissue (21). During breathing of pure O_2 after decompression, the N_2 pressure gradient is directed from the tissue to the alveolus. Although this pressure gradient creates a flux that tends to remove N_2 from the vicinity of the tissue bubble, N_2 still diffuses into the bubble, which enlarges (40). In our hypotheses, the relevant system in which thermodynamic forces act consists of two distinct spatial and functional subsystems. First, there is a microsystem consisting of tissue volume containing the bubble, its boundary layer, and a tissue shell. This microsystem then interacts with a macrosystem as the alveolus-arterial blood-tissue shell-venous blood serial cascade of structural or functional barriers. We then developed the FGM to explain how bubble growth is influenced by exercise-induced changes in the O_2 physiological resistances in series in both systems.

Because bona fide bubbles appear to form randomly (47, 50), we hypothesized that their spatial and temporal distributions in small units of tissue volume follow a Poisson process. Informally, the Poisson process asserts that the event of bubble formation occurs independently through time in any of a large number of small units of tissue volume, but with a small probability in any given unit at a given time (32, 38). This process is characterized by parameters that may depend on the type, intensity, duration, and chronology of exercise. At working altitude pressure, the total volume of all bubbles in tissue is propagated in time through the growth-and-decay mechanism, which applies independently for each bubble relative to its time of formation.

We demonstrated the potential mechanisms of exercise by applying the FGM in simulations to calculate total bubble volume for several variations of decompression procedures typical of actual EVAs. These variations were primarily characterized by differences in O_2 consumption, blood flow, and bubble formation rates (Poisson process). The results of our simulations suggested that exercise-induced elevation of O_2 consumption at altitude facilitated the persistence of bubbles in tissues, whereas exercise-enhanced perfusion tended to suppress bubble growth. The total volume of bubbles would be reduced unless increased tissue motion simultaneously raises the rate of bubble formation through cavitation processes, thus maintaining or increasing total bubble volume, despite the exercise.

Glossary

$(A\text{-}a)P_{O_2}(t)$	Alveolar-arterial P_{O_2} difference, Pa
$A_b(t)$	Surface area of the bubble at *time t*, m^2
α	Parameter of the Poisson process, dimensionless
$(a\text{-}\bar{v})P_{O_2}(t)$	Arterial-venous P_{O_2} difference, 8,000 Pa (~60 mmHg) at rest
β	Parameter of the Poisson process, dimensionless
D_i	Diffusivity of the *i*th gas species in the tissue, m^2/min
ϵ	Thickness of the diffusion barrier (protein layer), 2×10^{-6} m
FI_{O_2}	Fraction of O_2 in the inspired medium, dimensionless
h	Constant of proportionality = 2, dimensionless
J_N	Net flux of all gas species across the boundary layer, $mol \cdot m^{-2} \cdot min^{-1}$
J_i	Molar flux of the *i*th gas species across the boundary layer, $mol \cdot m^{-2} \cdot min^{-1}$
k_1	Tissue gas exchange rate constant for washin and washout of N_2, min^{-1}
k_2	Tissue gas exchange rate constant for washin and washout of O_2, min^{-1}
$M_b(t)$	Number of gas moles in the bubble, mol
$m_{CO_2}(t)$	Number of dissolved moles of CO_2 in the tissue, mol
$m_{H_2O}(t)$	Number of moles of water vapor from the tissue shell, mol
$m(t)$	Mean of the Poisson process, dimensionless
$M_{ti}(t)$	Number of gas moles in the tissue shell, mol
ν	Tissue elastic recoil from Ref. 14, 3.7×10^3 Pa (= 3.7×10^4 dyn/cm^2)
$N(t)$	Total number of bubbles in the *n* tissue units, dimensionless
$N_i(t)$	Number of bubbles formed in the *i*th unit at *time t*, dimensionless
Ω	Constant of proportionality estimated from Table 2, 0.87, dimensionless
P	Ambient pressure, Pa
$Pa_{d,O_2}(t)$	Partial tension of O_2 fraction dissolved in the arterial blood, Pa
$P_{A_i}(t)$	Alveolar partial pressure of gas *i*, Pa
$Pa_i(t)$	Arterial tension of gas *i*, Pa
$Pa_{Hb\,O_2}(t)$	Partial tension of O_2 fraction bound to Hb, Pa
$P_{b,i}$	Partial pressure of the *i*th gas in the bubble, Pa
$P_{b,mg}(t)$	Pressure of metabolic gases in the bubble, Pa
$P_{I_i}(t)$	Partial pressure of gas *i* in inspired breathing medium, Pa
Pti_i	Tissue tension of the *i*th gas, Pa
$P\bar{v}_i(t)$	Tension of gas *i* in the mixed venous blood, Pa
$P\dot{v}_{O_2}$	Tension drop of dissolved tissue O_2 due to O_2 consumption, Pa
$P\bar{v}_{O_2}$	Mixed venous P_{O_2}, Pa
$P_w(t)$	O_2 window, Pa
$\Psi_{O_2}(t)$	Arterial partial tension of dissolved O_2 that is not utilized in tissue metabolism, Pa
$\Phi_{O_2}(t)$	Overall O_2 pressure gradient in the macro- and microsystem, Pa

$\varphi_1(t)$	Sum of pressures due to surface tension and tissue elastic recoil, Pa
$\dot{Q}ti(t)$	Blood flow in the tissue shell, m^3/min
R	Universal gas constant, $N \cdot m \cdot mol^{-1} \cdot K^{-1}$
R	Respiratory exchange ratio: 0.7–1.12, 0.82 at rest, dimensionless
$R_b(t)$	Radius of a bubble at *time t*, m
$\bar{R}_b(t)$	Mean radius of bubbles from the entire region at *time t*, m
$\bar{R}_{b,max}$	Maximum mean radius of bubbles from *n* units at *time t*, m
R_q	Circulatory convective resistance, $Pa \cdot l^{-1} \cdot min$
$s_{b,i}$	Solubility of the *i*th gas in the blood, $ml \cdot ml^{-1} \cdot 100\ Pa^{-1}$
$s_{ti,i}$	Solubility of the *i*th gas in the tissue, $ml \cdot ml^{-1} \cdot 100\ Pa^{-1}$
τ	Surface tension of the tissue from Refs. 13 and 14, 10^{-2} N/m (= 10 dyn/cm)
T	Temperature, Kelvin
T	Total time of exposure to altitude, min
t	Time of interest measured from first pressure change (prebreathe), min
t_{alt}	Time of exposure to altitude immediately after decompression, min
$t_{b\ ij}$	Time of onset of the *j*th generated bubble in the *i*th unit of tissue volume measured from t_{alt} (t_{alt} = 0), min
$t_{1/2,N_2}$	Half time for tissue washin and washout of N_2, min
$t_{1/2,O_2}$	Half time for tissue washin and washout of O_2, min
$V_b(t)$	Volume of the bubble at *time t*, m^3
$V_{b\cdot}(t)$	Volume of bubbles in the tissue region, m^3
$V_{b\cdot max}$	Maximum volume of bubbles in the tissue region, m^3
v(t)	Intensity of the Poisson process, bubbles formed/min
$\dot{V}ti_{O_2}(t)$	O_2 uptake in the tissue shell, m^3/min
$Vti(t)$	Volume of the tissue shell at *time t*, m^3
$V_{tot}(t)$	Volume of the tissue element at *time t*, m^3
V_{tu}	Volume of the tissue unit (realized as a cube), m^3
x_i	Molar fraction of the *i*th gas species, dimensionless

METHODS

Growth-and-Decay Model for a Single Bubble

Macro- and microsystems of gas exchange. We define a tissue element to be a small spherical unit of tissue containing the bubble (Fig. 1*A*), where significant gas exchanges take place (4, 40). We assumed that every tissue element contains a single bubble and that the ratio of the volume of the tissue element (V_{tot}) to the bubble volume (V_b) is constant. The part of the tissue element that does not include the bubble per se will be referred to as the homogeneous tissue shell. We proceed to derive a differential equation relating the bubble radius (R_b), and hence V_b, to physical and physiological parameters obtainable from the characteristics of the decompression profile.

We consider two gas transport systems: a macrosystem, in which gases move from the alveolus to the tissue element and vice versa, and a microsystem for gas exchanges across the diffusion barrier inside the tissue element. In the macrosystem, CO_2 moves outward from the tissue element to the alveolus, and this flux is considered in the positive direction. Similarly, after decompression during breathing of N_2-O_2 mixtures, N_2 moves in the positive direction, from the supersaturated tissue element to the alveolus. In contrast, O_2 moves from the alveolus toward the tissue element, and the flux has a negative direction. Finally, water in the tissue fluid also tends to move toward the tissue element (negative direction) as it vaporizes to fill the empty space created by the forming bubble. In the microsystem (bubble-diffusion barrier-tissue shell), we establish signs for the gradient and flux of a gas across the diffusion barrier to be "positive" if it has same direction as the gas flux in the macrosystem (21, 28). During the initial explosive bubble growth phase, all gases in this system diffuse into the bubble (11). Thus CO_2 and N_2 have "negative" fluxes in this system, whereas O_2 has a positive flux. Water vapor diffuses into the de novo bubble; hence, it too has a positive flux in this system (Fig. 1*B*).

Diffusion of gases across the diffusion barrier in the microsystem. The volumes of gases are expressed under standard body conditions of temperature, ambient pressure, and saturated with water vapor (BTPS). In a three-dimensional coordinate system, the molar flux of the *i*th permeating ideal gas species (J_i) obeys Fick's first phenomenological law of diffusion (4, 14, 17, 18, 33, 39, 43) and can then be estimated by $J_i = -(P/RT)D_i\nabla x_i$, where P is the ambient pressure, R is the universal gas constant, T is the temperature in degrees Kelvin, D_i is the diffusion coefficient, and ∇x_i is the molar fraction gradient of the *i*th gas in the macrosystem. For air breathing, gas exchange dynamics involve four relevant species: CO_2, N_2, O_2, and H_2O ($i = 1, \ldots, 4$). In the macrosystem, ∇x_i is defined along a direct path to the center of the bubble, where the inward direction is negative and outward is positive. Resulting fluxes have signs in accordance with the "macrosystem" rule (inward = negative; outward = positive). In the microsystem, we establish that a flux is positive if it has the same direction as in the macrosystem (opposite direction = negative). Therefore, the CO_2 and N_2 fluxes are negative (Fig. 1*B*). The net flux (28) (J_N) into or out of the bubble is expressed as follows

$$J_N = -\frac{P}{RT}\sum_{i=1}^{4} D_i \nabla x_i \qquad (1)$$

Applying Henry's law to the dissolved tissue gases surrounding the bubble and using the ideal gas equations for gas pressures inside the bubble (14), $J_N(t)$ can be approximately expressed in terms of partial pressures of the *i*th gas as a function of time. As reported previously (14, 28), the net flux is thus expressed as follows

$$J_N(t) = -\frac{1}{RT\epsilon}\sum_{i=1}^{4} D_i[s_{ti,i}Pti_i(t) - P_{b,i}(t)] \qquad (2)$$

where $s_{ti,i}$ is the solubility of the *i*th gas species in the tissue element, ϵ is the thickness of the diffusion barrier, and $Pti_i(t)$ and $P_{b,i}(t)$ are the partial tissue tension and pressure within the bubble of the *i*th gas, respectively. When referring to a specific gas species, we use the convention of replacing the subscript *i* by the gas name (e.g., s_{ti,N_2} instead of $s_{ti,i}$). Time is

expressed in minutes and measured from the start of the prebreathe period to the end of the exposure to altitude. The prebreathe period begins at *time* $t = t_0 = 0$, when partial pressures of gases in the breathing medium start to change from the equilibrium of standard atmospheric conditions. Arrival at working altitude pressure (end of depressurization), occurs at *time* $t = t_{alt}$.

Moles of gas within the tissue shell and in the bubble. To evaluate the net flux (*Eq. 2*), we next calculate the number of moles of each gas crossing the diffusion barrier. Suppose a particular bubble forms at $t_b > t_{alt}$. For $t > t_b$, let $M_{ti}(t)$ be the total number of moles of gas in the tissue shell. From Henry's law (14), we have

$$M_{ti}(t) = \frac{s_{ti,N_2}}{RT} Vti(t) Pti_{N_2}(t) + \frac{s_{ti,O_2}}{RT} Vti(t) \Phi_{O_2}(t) + m_{CO_2}(t) + m_{H_2O}(t) \quad (3)$$

where $m_{CO_2}(t)$ and $m_{H_2O}(t)$ are the number of moles of dissolved CO_2 and water vapor, respectively, $Vti(t)$ is the tissue shell volume pertaining to the bubble at *time* t [which has been in existence for $(t - t_b)$ min], and $\Phi_{O_2}(t)$ is the O_2 overall pressure difference between the macro- and the microsystem. Using the equation of state of an ideal gas (14), we estimate the number of moles in the bubble

$$M_b(t) = \frac{V_b(t)}{RT} [P_{b,N_2}(t) + P_{b,CO_2}(t) + P_{b,O_2}(t) + P_{b,H_2O}(t)] \quad (4)$$

where $V_b(t)$ is the volume of the bubble at *time* t.

Estimation of the bubble radius. From the law of conservation of mass (21, 28), the number of moles diffusing into and out of the bubble per minute is

$$A_b(t) J_N(t) = \dot{M}_{ti}(t) - \dot{M}_b(t) \quad (5)$$

for $t > t_b$, where $A_b(t)$ is the surface area of the bubble and $\dot{M}_{ti}(t)$ and $\dot{M}_b(t)$ are gas mole uptake into and out of the tissue shell (microsystem) and into and out of the bubble, respectively. (We use the convention that the overdot denotes differentiation with respect to time.) By definition of the microsystem, we assume Vti to be proportional to V_b ($h = Vti/V_b \geq 1$) and h to be sufficiently small so that any gases entering or leaving the tissue shell are being involved in exchanges across the diffusion barrier of the microsystem. Finally, for $t > t_b$, *Eq. 5* can be rewritten in terms of the bubble radius $R_b(t)$

$$\dot{R}_b(t) = \frac{J(t) - \frac{1}{3} R_b(t)[h\dot{L}(t) - \dot{K}(t)]}{hL(t) - K(t)} \quad (6)$$

where $L(t)$ and $K(t)$ are quantities derived in the APPENDIX. For a given decompression profile, values of $K(t)$, $L(t)$, and $J_N(t)$ may be obtained as a function of time through measurements of inspired pressure and fraction of gases. Details of the calculation of $\dot{K}(t)$ and $\dot{L}(t)$ are given in the APPENDIX. *Equation 6* has no analytic solution for $R_b(t)$ and must be solved numerically.

Gas transport in the macrosystem: estimation of pressures and/or tensions. To obtain $L(t)$ and $K(t)$ in *Eq. 6*, it is first necessary to estimate the pressure gradients in the macrosystem. These may be calculated from values of the absolute pressure and inspired fractions of N_2 and O_2 and expired CO_2 in the breathing medium for each phase of our decompression profiles. In addition, within the macrosystem, we consider partial pressures of each gas: inside the alveolus [$P_A(t)$], inside the pulmonary capillary [$Pa(t)$], and in the mixed venous blood [$P\bar{v}(t)$]. For all gases, we assume $P\bar{v}(t) = Pti(t)$.

N_2 tissue tension. On the downstream side of the macrosystem flow, we estimated Pti_{N_2} for $t > t_{alt}$ using the classical exponential equation (8, 11, 14). Using this method, we computed Pti_{N_2} by increments at fixed times $t_1, t_2, \ldots, t_n$, where $t_{n-1} = t_{alt}$ and $t_n = t$. The incremental expression for Pti_{N_2} is given by

$$Pti_{N_2}(t_j) = Pa_{N_2}(t_j) + [Pti_{N_2}(t_{j-1}) - Pa_{N_2}(t_j)] e^{-k_1(t_j - t_{j-1})} \quad (j = 1, 2, \ldots, n) \quad (7)$$

where Pa_{N_2} is the N_2 arterial tension derived from the alveolar gas equations and partial pressures (11, 42) and k_1 is the tissue gas exchange rate constant for N_2.

O_2 transport. On the upstream side of the macrosystem flow portrayed in Fig. 1*B*, O_2 is driven through a series of interfaces (12) into the tissue element, where it is dissolved. To correctly model the flow, it is necessary to estimate pressure differences across various encountered interfaces as follows (Fig. 1*C*). First, because of the alveolar membrane, there is an alveolar-arterial pressure difference [$(A\text{-}a)PO_2(t)$], which tends to increase with $PI_{O_2}(t)$ (5, 15, 37). On the basis of our own measured values of $PI_{O_2}(t)$, we estimated $(A\text{-}a)PO_2(t)$ with an algorithm that uses values given by Clark and Lambertsen (5). We then obtained $Pa_{O_2}(t)$ by subtraction from $PA_{O_2}(t)$. Second, the O_2 transfer to the capillaries occurs when O_2 is transported in physical solution or bound to Hb. Above the threshold $Pa_{O_2}(t)$ of 13.33 kPa (100 Torr, 1 kPa = 7.50062 Torr), the O_2 saturation is assumed to be 100% and the unbound O_2 remains in physical solution. In terms of tension, the arterial O_2 tension is made up of two components, the O_2 dissolved fraction [$Pa_{d,O_2}(t)$] and the Hb-bound O_2 [$Pa_{Hb\,O_2}(t)$]. We used an algorithm derived from the O_2 dissociation curve (29, 35, 36) to estimate $Pa_{Hb\,O_2}(t)$ as a function of $Pa_{O_2}(t)$. Third, the O_2 supply to the mitochondria results in the withdrawal of O_2 from further utilization in the O_2 transport process across the bubble boundary layer. Di Prampero and Ferretti (9, 10) derived a relationship between the O_2 tissue consumption [$\dot{V}ti_{O_2}(t)$] and the arteriovenous O_2 difference [$(a\text{-}\bar{v})PO_2(t)$]. The relationship is $\dot{V}ti_{O_2}(t) = [(a\text{-}\bar{v})PO_2(t)]/R_q = P\dot{v}_{O_2}(t)/R_q$, where R_q is the circulatory convective resistance and $P\dot{v}_{O_2}$ is the tension drop of dissolved tissue O_2 due to O_2 consumption. Finally, O_2 supplied to the tissue element can potentially participate in bubble gas exchanges of the microsystem. Thus the tension of the dissolved O_2 that is applied to the microsystem at *time* t [$\Psi_{O_2}(t)$] can be written in the form

$$\Psi_{O_2}(t) = Pa_{O_2}(t) - Pa_{Hb\,O_2}(t) - P\dot{v}_{O_2}(t) \quad (8)$$

Dissolution of O_2 in the tissue element follows Henry's law and is described by an exponential relation similar to *Eq. 7*. As was the case for N_2, $\Phi_{O_2}(t)$, the overall O_2 pressure gradient in the macro- and microsystem that applies from the alveolus to the tissue element can be expressed incrementally at fixed times $t_1, t_2, \ldots, t_n \equiv t$, so that

$$\Phi_{O_2}(t_j) = \Psi_{O_2}(t_j) + (A - a)PO_2(t_j) + [\Phi_{O_2}(t_{j-1}) - \Psi_{O_2}(t_j) + (A - a)PO_2(t_j)] e^{-k_2(t_j - t_{j-1})} \quad (9)$$

where k_2 is the tissue gas exchange rate constant for O_2. Indeed, metabolism lowers the O_2 tension in the tissue element below Pa_{O_2}, creating a phenomenon known as the "O_2 window" or "inherent unsaturation" (11, 16, 23, 34, 42). The sum of partial tensions of the dissolved gases in the tissues is usually less than atmospheric pressure. The O_2 window [$P_w(t)$] is calculated by subtracting the sum of pressures of all dissolved gases to the ambient pressure and can be written using $\Phi_{O_2}(t)$ so that $P_w(t) = \Phi_{O_2}(t) + \{P(1 - F_{IO_2}) - [Pti_{N_2}(t) +$

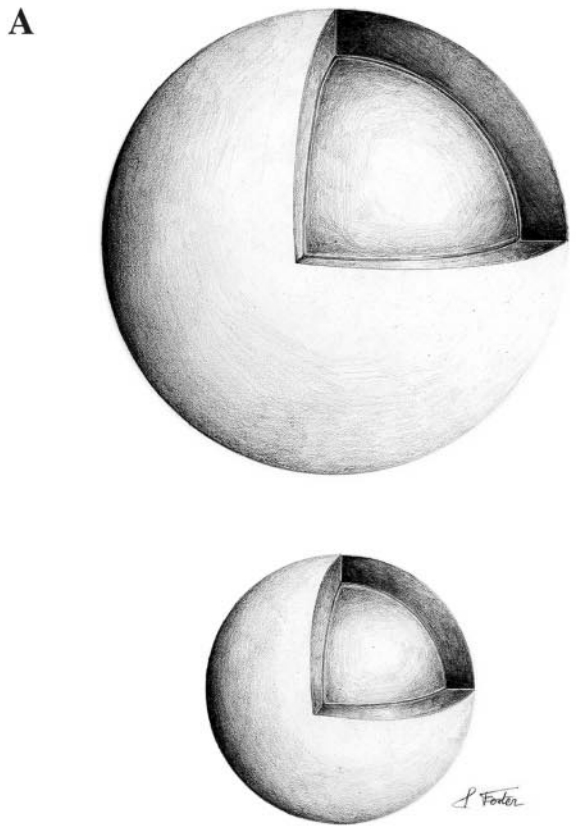

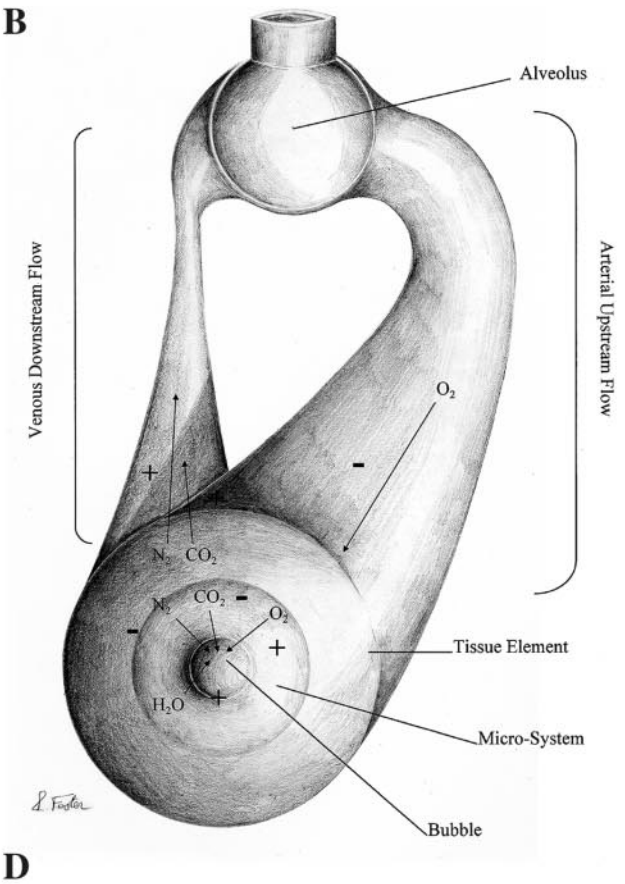

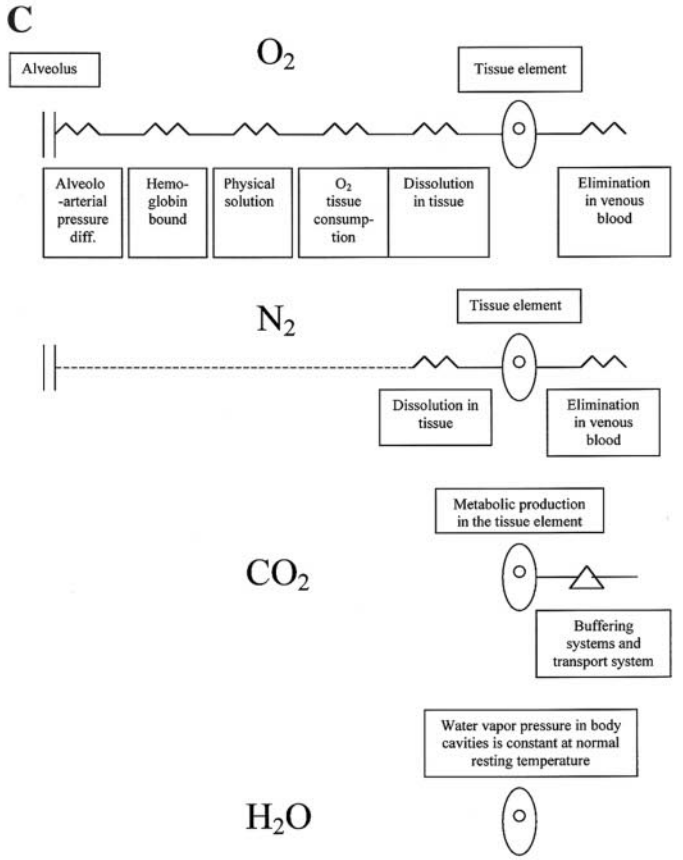

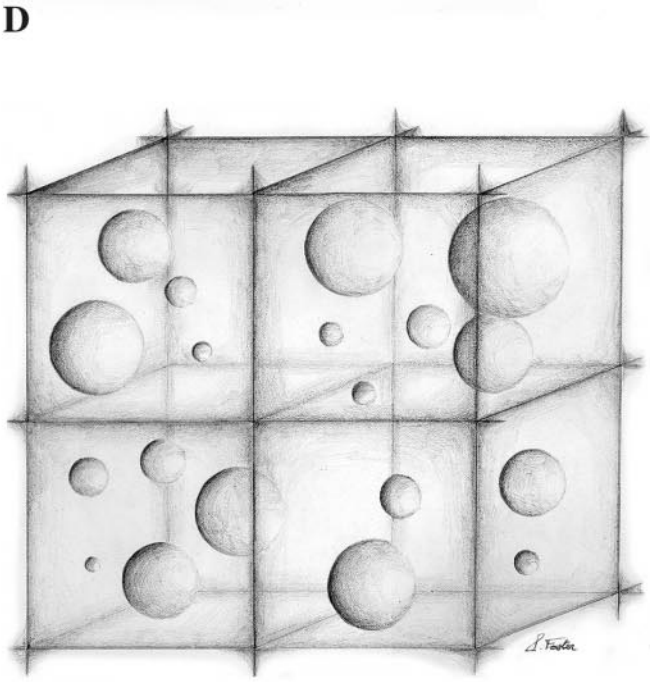

$Pti_{CO_2}(t) + Pti_{H_2O}(t)]\}$. *Equations 7* and *9* are then used in the APPENDIX to calculate $L(t)$ and $K(t)$.

Number and onset times of bubbles in tissue. Yount (50) proposed a stochastic model for accretion and deletion of skin molecules that leads to an exponential distribution for the number of micronuclei. Here, we consider a stochastic model of bubble formation in which micronuclei evolve into bubbles at random times after decompression following a Poisson process. Consider a tissue region divided into n units of tissue that are identical in makeup and perfusion (40). Each tissue unit is independent, and there is no diffusion from one unit to another. All tissue units are the same size, and units are evenly distributed in space. In contrast, bubbles in one unit are of different age and size. Schematically, the units are illustrated as cubes of constant volume V_{tu} in Fig. 1*D*. For a total time at altitude of T minutes, $N_i(t)$ (i = 1, . . . , n), the number of bubbles formed in the *i*th unit of tissue volume up to *time t* (in minutes, $0 < t \leq T$) is assumed to follow a nonhomogeneous Poisson process (32, 38) with intensity $v(t)$, $v(t) = \alpha e^{-\beta t}$. The parameters α and β are driven by the decompression procedure and the level of exercise or rest. For a given procedure, α also serves as a scaling factor, being proportional to V_{tu}. The decreasing exponential form of $v(t)$ reflects the rapidly decreasing propensity to form bubbles as exposure time increases (6, 22).

To be a Poisson process, $N_i(0) = 0$, $N_i(t)$ must have independent increments; i.e., the number of bubbles formed in nonoverlapping intervals of time must be statistically independent, and two or more bubbles cannot form simultaneously. Physically, the latter two requirements correspond to temporal and spatial independence of bubble formation. It can be shown under these assumptions (32) that $N_i(t)$ has a Poisson distribution with mean

$$m(t) = \int_0^t \nu(u)du = \frac{\alpha}{\beta}(1 - e^{-\beta t}) \qquad (10)$$

In other words, the probability p to obtain k bubbles up to *time t* is $p[N_i(t) = k] = \exp[-m(t)][m(t)]^k/k!$ (k = 0, 1, . . .).

Mean bubble radius and total volume of bubbles. The mean bubble radius for the given region of tissue at *time t* can be written as

$$\bar{R}_b(t) = \frac{1}{N(t)} \sum_{i=1}^{n} \sum_{j=1}^{N_i(t)} R_{b,ij}(t) \qquad (11)$$

where $N(t) = \sum_{i=1}^{I} N_i(t)$ and $R_{b,ij}(t)$ is the radius of the *j*th bubble in the *i*th tissue unit. By convention, we take $R_{b,ij}(t) =$ 0 if the bubble has not formed by *time t*. Under the additional assumption that bubbles form and grow independently over the *n* tissue units, $N(t)$ is also a Poisson process (32, 38). If the region is homogeneous in the sense that all the Poisson processes $N_i(t)$ have identical values of α and β, then the mean of $N(t)$ is simply $(n\alpha/\beta)(1 - e^{-\beta t})$. With the assumption of spherical bubbles, the total volume of bubbles in the region of tissue at *time t* is

$$V_{b.}(t) = \frac{4}{3}\pi \sum_{i=1}^{n} \sum_{j=1}^{N_i(t)} R_{b,ij}^3(t) \qquad (12)$$

Experimental Design

We applied the FGM to four types of decompression profiles (*A–D*) typical of chamber tests and actual EVAs (Table 1). These profiles shared the following properties: *1*) the duration of prebreathe was 210 min (P = 101.13 kPa, FI_{O_2} = 1); *2*) ascent time was 6 min; and *3*) $FI_{O_2} = 1$. The altitude pressure was 30 kPa for *profiles A–C* compared with 60 kPa for *profile D*. In *profiles A* and *D*, physiological parameters $P\dot{v}_{O_2}$, R, $t_{1/2,N_2}$, and $t_{1/2,O_2}$ were set to known values of 8 kPa, 0.82, 360 min (7), and 313.2 min, respectively. These values are consistent with the case of no exercise. In addition, $t_{1/2,O_2}$ was calculated using *Eq. A13*. Using experimental data, we found in another study (11a) that the Poisson process parameter $\beta = 0.017$ for profiles without prebreathe exercise but with mild exercise (817 kJ) at altitude. We assumed that, for a control case of no exercise at any time, β would be reduced by 20% (to ~0.014), reflecting the decreased propensity to form bubbles. In contrast, *profile B* incorporated mild exercise at altitude to emulate the moderate workloads performed by astronauts during ordinary EVA. For this case, we assumed $P\dot{v}_{O_2}$ = 10 kPa, R = 0.95, $t_{1/2,N_2}$ = 200 min, and $t_{1/2,O_2}$ = 174 min. *Profile C* also simulates exercise, but with two phases (10 min of heavy exercise followed by 25 min of light exercise) during prebreathe. Physiological parameters were set at $P\dot{v}_{O_2}$ = 12 kPa, R = 1.12, $t_{1/2,N_2}$ = 60 min, and $t_{1/2,O_2}$ = 52.2 min (phase 1) and then at $P\dot{v}_{O_2}$ = 10 kPa, R = 0.95, $t_{1/2,N_2}$ = 80 min, and $t_{1/2,O_2}$ = 69.5 min.

For each profile type, various simulations of bubble formation and growth were analyzed to examine the effect of exercise on $\bar{R}_b(t)$ and $V_{b.}(t)$. For *simulations A9–A11* (Table 1), we modified values of $P\dot{v}_{O_2}$ while keeping all other parameters fixed to isolate the effect of $\dot{V}ti_{O_2}$. These higher values are representative of heavier exercise workloads required to perform EVA tasks during some orbital missions. For *simulations A7* and *A8*, β was increased by a factor of 3 to emulate

Fig. 1. *A*: views of the microsystem for 2 bubble sizes. The bubble is coated with a thin adsorbed protein layer, which is a barrier for the diffusion of gases into and out of the bubble. The spherical tissue shell surrounding the coated bubble of volume V_{tot} is proportional to the bubble volume (V_b) and continually redefined as the bubble grows or decays ($V_{tot} = hV_b$). We assume that h = 2. *B*: periphery of spherical tissue element (part of the macrosystem) envelops the microsystem, an imaginary smaller and inner spherical volume without any real interface. The microsystem contains the bubble and the surrounding tissue shell, which is sufficiently small so that any gas moles entering or leaving the tissue shell are also involved in exchanges across the bubble diffusion barrier. Movement of gas is illustrated by arrows. Direction of gas fluxes during the initial explosive bubble growth phase is shown; later during decay, flux directions of certain gas species may be reversed. Sign (+ or −) of gas flux is obtained according to the rule described in METHODS. *C*: pressure gradients and structural and functional barriers. Six O_2 physiological resistances in series modify the O_2 pressure gradient to the bubble (*Eq. 9*). In the case of N_2, only 2 functional barriers, the tissue dissolution and elimination, are critical (*Eq. 7*). Because we simulate submaximal levels of exercise, the total content of CO_2 increase in the tissue should not exceed the removal capacity by blood flow. Therefore, we derived our equations for a constant P_{CO_2} in tissue of 6.13 kPa (46 mmHg). *D*: tissue region is made up of *n* identical and homogeneous volumes, the units of tissue volume. Four of these units are pictured by cubes that contain bubbles. In each unit of tissue volume, bubbles of different age and size follow a Poisson distribution. Mean for the Poisson distribution is 6.

Table 1. *Simulated decompression profiles*

Simulation	Altitude, kPa	Exercise	$P\dot{v}_{O_2}$, Pa	R	$t_{1/2,N_2}$, min	$t_{1/2,O_2}$, min	α	β	$\bar{R}_{b,max}$, μm	$V_{b\cdot max}$, mm^3
				No exercise						
A1	30	No	8.0	0.82	360	313.2	0.084	0.014	34.14	
A2	30	No	8.0	0.82	360	313.2	0.102	0.017	44.52	
A3	30	No	8.0	0.82	360	313.2	0.084	0.014	35.46	
A4	30	No	8.0	0.82	360	313.2	0.102	0.017	44.6	
A5	30	No	8.0	0.82	360	313.2	0.084	0.014		0.049
A6	30	No	8.0	0.82	360	313.2	0.102	0.017		0.086
				Poisson parameters of exercise, physiological parameters at resting values						
A7	30	Altitude*	8.0	0.82	360	313.2	0.252	0.042	47.5	
A8	30	Altitude*	8.0	0.82	360	313.2	0.306	0.051	49.79	
				O_2 consumption at exercise values, other parameters at resting values						
A9	30	Altitude*	12	0.82	360	313.2	0.084	0.014	35.74	
A10	30	Altitude*	18	0.82	360	313.2	0.084	0.014	38.19	
A11	30	Altitude*	20	0.82	360	313.2	0.084	0.014	38.88	
				All parameters have exercise values						
B1	30	Altitude	10	0.95	200	174.0	0.084	0.014	12.42	
B2	30	Altitude	10	0.95	200	174.0	0.102	0.017	16.18	
B3	30	Altitude	10	0.95	200	174.0	0.9	0.036		0.0464
B4	30	Altitude	10	0.95	200	174.0	0.94	0.0376		0.0498
B5	30	Altitude	10	0.95	200	174.0	0.95	0.038		0.0495
B6	30	Altitude	10	0.95	200	174.0	0.9625	0.0385		0.0502
B7	30	Altitude	10	0.95	200	174.0	1.025	0.041		0.052
B8	30	Altitude	10	0.95	200	174.0	1.2	0.048		0.056
B9	30	Altitude	10	0.95	200	174.0	1.375	0.055		0.058
B10	30	Altitude	10	0.95	200	174.0	1.75	0.07		0.065
B11	30	Altitude	10	0.95	200	174.0	2.5	0.1		0.074
B12	30	Altitude	10	0.95	200	174.0	5	0.2		0.087
B13	30	Altitude	10	0.95	200	174.0	17.5	0.7		0.1
B14	30	Altitude	10	0.95	200	174.0	37.5	1.5		0.1
				Exercise during prebreathe						
C1	30	Prebreathe	12 & 10	1.12–0.95	60–80	52.2–69.5	0.084	0.014	6.05	
C2	30	Prebreathe	12 & 10	1.12–0.95	60–80	52.2–69.5	0.102	0.017	7.28	
				Lower altitude, no exercise						
D1	60	No	8.0	0.82	360	313.2	0.084	0.014	20.76	

*Some parameters have values of exercise at altitude. See *Glossary* for definitions of abbreviations.

the effect of an increased rate of bubble formation, but with physiological parameters remaining at no-exercise levels. This would be the case if mechanical motion takes place without significant additional O_2 consumption. It has been conjectured that mechanical motion of tissues may cause cavitation (19) and increase the bubble formation rate (20). For simulations involving *profiles A, C*, and *D*, the parameter α was chosen to make the expected number of bubbles per tissue unit ($\approx \alpha/\beta$) equal to 6.0 over 50 tissue units.

For the case of exercise at altitude (*simulations B1–B14*), we investigated the effect of bubble formation rate on maximum bubble volume. This rate was again controlled by varying β. During this exercise, more units of tissue would be recruited for bubble formation; therefore, we increased n, the number of tissue units, to 100. Also, the density of bubbles per tissue unit would be expected to be greater than at rest; hence, we changed α so that the mean number of bubbles per unit was 25.

Simulation Process

An overview of the simulation is illustrated in Fig. 2. Working values of solubilities of gases (N_2, O_2, and CO_2) in the tissue element were chosen to lie in the range of similar values for blood (Table 2). Diffusivities of gases were chosen as ~75% of corresponding values for water (Table 2) and 200% of the values for lipids. Values of other physical constants are listed in the *Glossary*.

From the Poisson distribution with mean m(t) (*Eq.* 10), we generated $N_i(T)$, the total number of bubbles formed over a decompression period of T minutes. Values of α and β defining m(t) are given in Table 1. Methodology for generating random numbers from the Poisson distribution is well known (32). Next, we used a property of Poisson processes (32) that relates the conditional distribution of event times to the mean, when the total number of events is known. This enabled us to generate random bubble creation times $t_{b,ij}$ [j = 1, . . . , $N_i(T)$; see APPENDIX].

For each creation time, *Eq. 6* was constructed using *Eqs. 1–5* and *A1–A13,* where t_b in the APPENDIX is replaced by $t_{b,ij}$, i.e., onset time of the jth bubble in the ith unit of tissue volume. Numerical solutions $R_{b,ij}(t)$ for $R_b(t)$ in *Eq.* 6 were then found for each simulated bubble radius at 10-min intervals using Mathematica software version 3.0.1 (49). Solution of *Eq. 6* proved difficult. In general, a combination of nonstiff

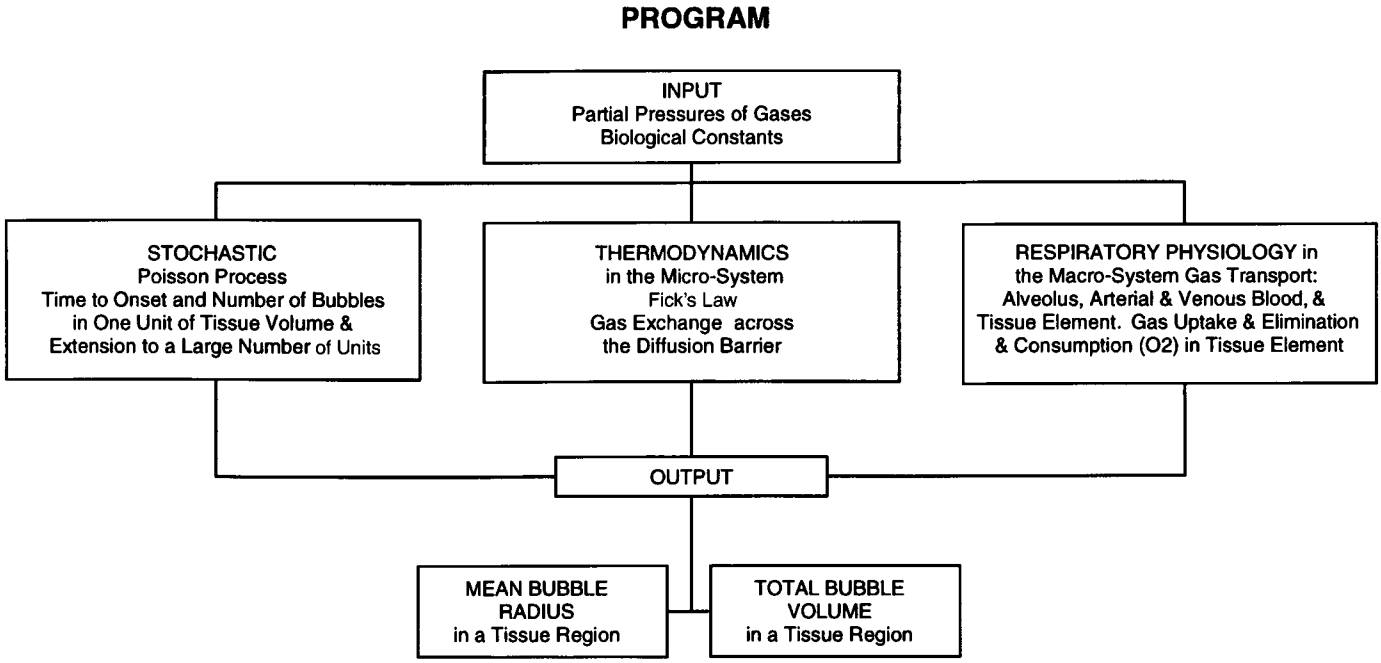

Fig. 2. Simulation flow chart.

Adams or stiff Gear, Fehlberg order 4–5, or Runge Kutta methods for nonstiff equations was required to achieve convergence. The Gel'fand-Lokutsiyevski chasing method was used for solving the boundary value problem. Processing of 300 bubbles took ~2 min to run on a 300-mHz personal computer with 64 MB of random access memory. Finally, the $R_{b,ij}(t)$ was used in *Eqs. 11* and *12* to calculate $\bar{R}_b(t)$ and $V_b(t)$.

RESULTS AND DISCUSSION

Effects of O_2 Consumption on Bubble Dynamics

Simulations A1 and *A9–A11* were run with different levels of O_2 consumption at altitude ($P\dot{v}_{O_2}$ = 8, 12, 18, and 20 kPa) with bubble formation parameters (α and β) and blood flow fixed at resting control values (Table 1). Bubble growth to $\bar{R}_{b,max}$ was essentially the same for all four levels of O_2 consumption. These results are consistent with those of Van Liew et al. (42), who noted that a large O_2 window, especially during O_2 breathing, reduced the bubble enlargement. They also reported no significant change in the O_2 window values at arteriovenous pressure differences <100 kPa (FI_{O_2} = 1). Similarly, we observed that increasing O_2 extraction ($P\dot{v}_{O_2}$ > 9 kPa) had little or no effect on the O_2 window, and therefore maximal bubble growth was not affected. However, the average bubble size decreased slowly in time when $\dot{V}ti_{O_2}$ increased, whereas low resting $\dot{V}ti_{O_2}$ values facilitated faster decay (Fig. 3*A*). Because O_2 has a greater permeation coefficient than N_2, short transients of O_2 permeate rapidly into the bubble at rest [$P\dot{v}_{O_2}(t)$ = 8 kPa]; simultaneously, N_2 exits the bubble to the surrounding tissue (40). Then, O_2 rapidly permeates out of the bubble, resulting finally in a rapid bubble decay. In contrast, tissue O_2 extraction is enhanced during exercise; thus a relatively small amount of O_2 diffuses into the bubble and is exchanged for N_2. Therefore, N_2 builds up in the bubble, which in turn reduces the bubble decay rate.

Table 2. *Physical constants in the tissue*

	N_2	O_2	CO_2
Solubilities, ml·ml^{-1}·100 kPa^{-1}	0.0150	0.020	2.10
Diffusivities, cm^2/min	1.0×10^{-3}	9.3×10^{-4}	7.9×10^{-4}

Solubilities in the tissue element are in the range of similar values for blood (3, 4, 14, 18, 24, 39, 42, 46). Diffusivities are ~75% of corresponding values for water and 200% of values for lipids.

Exercise Decreases the Mean Bubble Radius

Aerobic exercise-enhanced blood flow, before and/or after decompression, generates a cascade of events in the macro- and microsystem as follows. Augmentation of blood flow [$\dot{Q}ti(t)$; *Eq. A12*] causes a decrease in the O_2 and N_2 tissue washin and washout half times, $t_{1/2,i} = (\ln 2)/k_i$, where k_i is the tissue gas exchange rate constant. As a result, excess N_2 in the tissue element is carried away before it can diffuse into postdecompression bubbles. The fast N_2 removal by blood precludes bubble enlargement (40). Also, little or no N_2 is carried to the tissue when breathing enriched O_2 mixtures. In contrast, a greater amount of O_2 physically dissolves in the tissue element, which in turn moderately reduces the O_2 window.

Hills and LeMessurier (16) reported that, after 15 min of exposure of rabbits to an hyperoxic medium, the O_2 window was large. Here, we agree that only a small amount of O_2 would dissolve in the tissue during this time interval. However, during several hours of hyperoxic O_2 prebreathe/altitude exposure, greater amounts of O_2 would dissolve in tissues, thereby eventually reducing the O_2 window. According to Lambertsen et

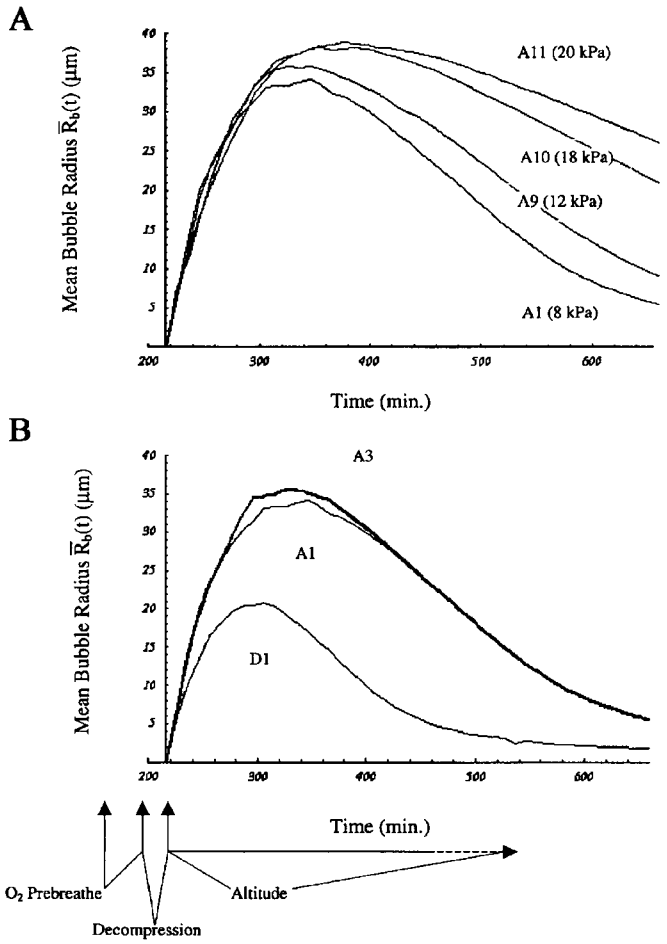

Fig. 3. Simulations of $\bar{R}_b$ in various conditions. Time is measured from the start of prebreathe period and the elapsed time until altitude exposure begins at 216 min. Some bubbles start to grow on arrival at altitude. *A*: simulations of decompression *profile A* under 4 levels of O_2 consumption, i.e., $P\dot{v}_{O_2}$ at 8 kPa (*A1*), 12 kPa (*A9*), 18 kPa (*A10*), and 20 kPa (*A11*); as $\dot{V}ti_{O_2}$ (and $P\dot{v}_{O_2}$) increases, bubbles decay less rapidly. *B*: effect of the O_2 window. At an altitude exposure of 60 kPa (*D1*, FI_{O_2} = 1), a large O_2 window suppresses bubble growth. Two realizations (*A1* and *A3*) of *profile A* (no exercise) show very little difference in $\bar{R}_b$; variance due to the Poisson process is minimal and does not significantly impact interpretation of the results. See *Glossary* for definition of abbreviations.

al. (23), other mechanisms such as hypercapnic vasodilatation may also facilitate the O_2 transfer to the tissue, which in turn accelerates the window reduction. Lambertsen et al. also showed in humans, that arterial hypercapnia, a highly potent vasodilator of cerebral blood vessels, in conjunction with breathing for 15 min at 3.5 atm (fraction of CO_2 in the inspired medium = 0.02, FI_{O_2} = 0.98) induced a significant elevation of $P\bar{v}_{O_2}$ (146 kPa) in internal jugular venous blood samples, as compared with breathing without hypercapnia (FI_{O_2} = 1, $P\bar{v}_{O_2}$ = 10.13 kPa). In both cases Pa_{O_2} = 266 kPa; however, hypercapnia via cerebral vasodilatation reduced the O_2 window in very limited time.

Observations in pigs breathing hyperoxic mixtures showed that the bubble incidence in the pulmonary artery was reduced as Pa_{O_2} increased (34). Here, for pure O_2 breathing, we illustrate how P = PI_{O_2} affects $\bar{R}_b(t)$ through change in Pa_{O_2}. Figure 3*B* shows $\bar{R}_b(t)$ for the case of no exercise at two different altitudes: P = 30 kPa (*simulation A1*) and P = 60 kPa (*simulation D1*). At 60 kPa, the larger value of Pa_{O_2} induces a significant reduction in $\bar{R}_{b,max}$. Therefore, we postulate that the O_2 window inhibits bubble enlargement at the beginning of the altitude exposure. Later, because of increased perfusion, the higher O_2 flow to tissues augments the amount of dissolved O_2 in the unit of tissue volume. This, in turn, decreases the O_2 window, thus tending to slow the rate of bubble decay. However, the greater amounts of physically dissolved O_2 facilitate increased O_2 exchange within the microsystem. According to Van Liew and Burkard (41), many short O_2 transients would permeate rapidly in the bubble, resulting finally in a marked decay rate of bubble radii.

Figure 4 compares $\bar{R}_{b,max}$ for decompression profiles whose physiological parameters ($P\dot{v}_{O_2}$, R, $t_{1/2,N_2}$ and $t_{1/2,O_2}$) have the characteristics of no exercise, moderate exercise at altitude, and heavy exercise during prebreathe, but where β is held fixed. First, we compared the effect of exercise when β is set to the resting value of 0.014 (*simulations A1, B1*, and *C1*). Then a similar comparison was made for β = 0.017 (*simulations A2, B2*, and *C2*). For both values of β, we observed that $\bar{R}_{b,max}$ dropped by ~64%, (from 34.1 to 12.4 μm for β = 0.014 and from 44.5 to 16.2 μm for β = 0.017). When the effect of heavy exercise during prebreathe was compared with the case where there is no exercise, the drop was more dramatic, i.e., ~83% for both values of β. Results of these simulations illustrate how an augmentation of blood flow, which decreases $t_{1/2,N_2}$ and $t_{1/2,O_2}$, is paralleled by a reduction of bubble radius

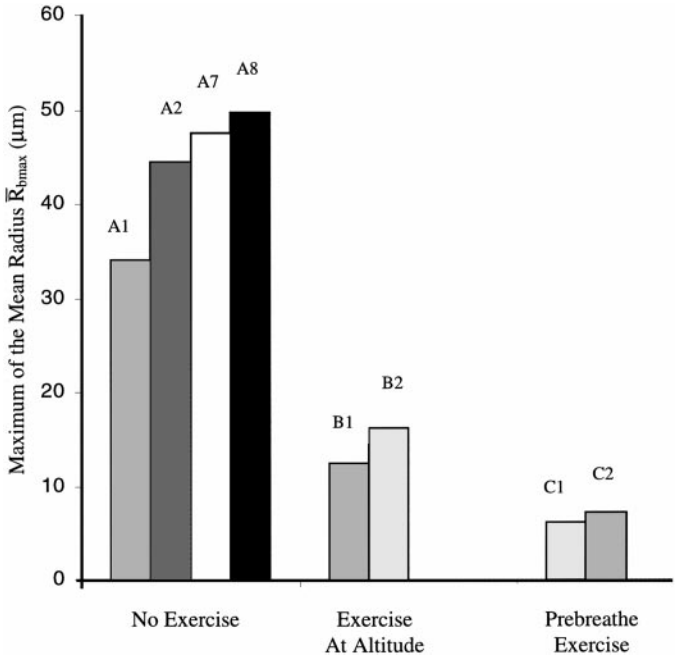

Fig. 4. Maximum bubble growth in various conditions of rest and exercise. Simulations of no exercise (*A1, A2, A7*, and *A8*), exercise at altitude (*B1* and *B2*), and heavy exercise during prebreathe (*C1* and *C2*) are shown.

regardless of the intensity of the Poisson process and the level of $\dot{V}ti_{O_2}$.

Also, with an acceleration of the nucleation process (β increased from 0.014 to 0.017), the increase in $\bar{R}_{b,max}$ was much more pronounced for the no-exercise case than for the case of exercise at altitude. However, the relative increase was about the same (30%), and for the prebreathe case the relative change appeared less (~20%). This is probably because, regardless of the nucleation rate, only small amounts of dissolved N_2 remain to be available for bubble growth after the start of decompression.

For *profile A*, we investigated the effect of increasing β from its resting value of 0.014 to large values reflecting intense bubble formation with physiological parameters remaining fixed ($P\dot{v}_{O_2}$ = 8 kPa, R = 0.82, $t_{1/2,N_2}$ = 360 min and $t_{1/2,O_2}$ = 313.2 min). We observed that in *simulations A1, A2, A7,* and *A8*, $\bar{R}_{b,max}$ increased from 34.1 to 49.8 μm as β increased from 0.014 to 0.051 (Fig. 4). As β increases, early formation of bubbles before N_2 supersaturation drops, leading to larger radii than the resting case (*simulation A1*). The pattern of increase was nonlinear, tending toward a plateau for large values of β. This is because, no matter how early the bubble is formed, for a fixed N_2 pressure gradient, the amount of N_2 available for diffusion into a bubble is limited.

Does Exercise at Altitude Increase the Volume of Tissue Bubbles?

In general, it has been observed that there is an increased incidence of DCI symptoms for subjects exercising at altitude after decompression (20). However, a diving experiment showed that exercise during decompression actually reduced Doppler-detectable venous gas emboli (19). Therefore, it is unclear how exercise affects the incidence of tissue bubbles. Using the FGM, we evaluated the effect of exercise in terms of how much the bubble formation process would have to be accelerated to achieve a value of $V_{b\cdot max}$ equal to that in a no-exercise case. For example, *simulations A5* (no exercise) and *B5* (exercise at altitude) produced about the same value of $V_{b\cdot max}$ (0.049 mm^3). In the latter case, β had to be increased by a factor of ~2.5 (from 0.014 to 0.38) to achieve the same $V_{b\cdot max}$. In other words, ~9.5 times as many bubbles would have to be generated with exercise at altitude to achieve the same maximum volume as at rest. Despite similar values of $V_{b\cdot max}$, $V_b(t)$ differed considerably. For the exercise case (*simulation B5*), a relatively large number of smaller bubbles formed earlier, whereas in the no-exercise case (*simulation A5*), larger bubbles were formed, but mostly at later times (Fig. 5*A*).

As demonstrated in Fig. 4, exercise-enhanced blood flow reduces $\bar{R}_{b,max}$ and, therefore, $V_{b\cdot max}$ for a fixed number of bubbles formed. In this case, the only way $V_{b\cdot max}$ could be increased is through a more intense generation of bubbles. In *simulations B3–B14*, we calculated $V_{b\cdot max}$ for *simulation B* (exercise at altitude), with β ranging from 0.036 to 1.5. In Fig. 5*B*, $V_{b\cdot max}$ increases rapidly as a function of β when β is small and reaches a plateau of ~0.1 mm^3 for β > 0.3. The reason is that, similar to the no-exercise case, the N_2 pressure gradient limits the supply of N_2 available for bubble growth in the tissue region.

Stability

We found that varying the initial minimal value of the bubble radius, within a range of 10^{-8}–10^{-4} m, did not affect the bubble growth dynamics; thus it appears that the differential *Eq. 6* is stable, and therefore, our model is robust with respect to the choice of the size of micronuclei. Also, the variability (<2.3%) inherent in the Poisson process did not affect the reproducibility of

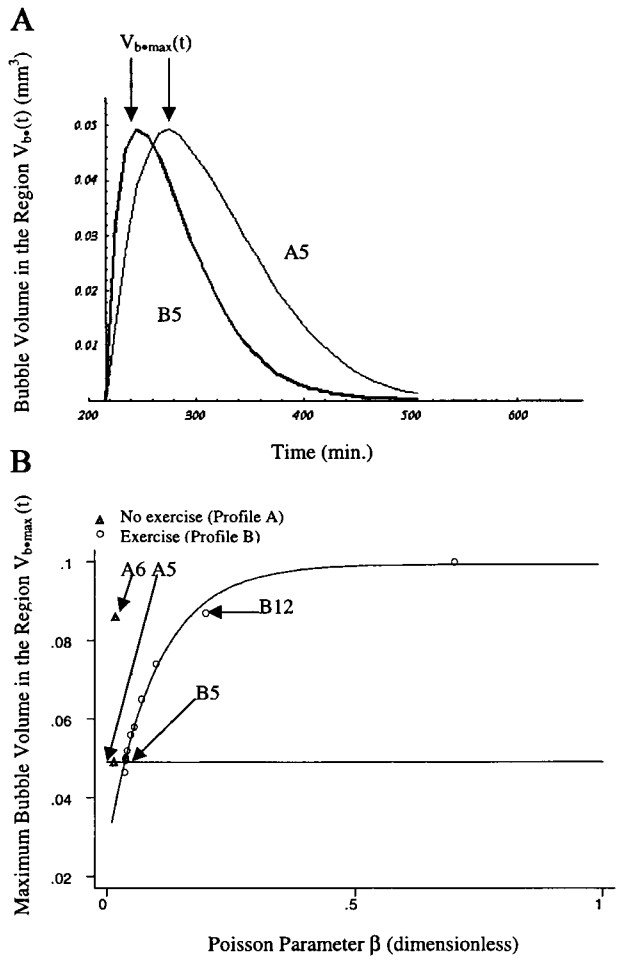

Fig. 5. *A*: effect of exercise at altitude on total volume of bubbles. *A5,* no exercise; *B5,* exercise at altitude. To achieve the same $V_{b\cdot max}$ as at rest [N(*t*) = 274], β had to be increased by a factor of ~2.5 (from 0.014 to 0.38), resulting in ~9.5 times as many bubbles as with exercise at altitude [N(*t*) = 2,612]. For *B5*, a relatively large number of smaller bubbles formed earlier; for *A5*, larger bubbles were formed, but mostly at later times. Therefore, $V_{b\cdot max}$ for *A5* was shifted to the right. *B*: limitation of the maximal bubble volume produced in the tissue region. In *simulations B3–B14*, we calculated $V_{b\cdot max}$ for *profile B* (exercise at altitude), with β ranging from 0.036 to 1.5. $V_{b\cdot max}$ increases rapidly as a function of β when β is small and reaches a plateau of ~0.1 mm^3 for β > 0.3. β had to be increased by a factor of ~11.7 (β = 0.2) in *simulation B12* to achieve the same $V_{b\cdot max}$ as in *simulation A6* (β = 0.017).

the simulation results for various realizations of the same profile. *Simulations A1* and *A3* represent two realizations of *profile A* (no exercise). As shown in Fig. 3*B*, there is very little difference in $\bar{R}_b(t)$ between these two examples. As a further illustration of variability, we found that $\bar{R}_{b,max}$ varied with a standard deviation of ~1.6% over 13 similar realizations. Also, the time of maximum bubble radius varied with a standard deviation of ~3%. However, this small amount of variation does not explain the different decompression outcomes observed over a population of subjects. Significant variability may be associated with age, body mass index, time of the day, seasonal variation, body temperature, body chemistry, and previous injuries (2).

Review of Assumptions

Physical parameters, e.g., $s_{ti,i}$, D_i , ν, ,τ, ϵ, and h, were selected only for a hypothetical tissue derived as a mixture of known values (3, 4, 14, 24, 41, 46) for blood and lipids. In reality, values of these parameters would be expected to vary for a given subject over time and also between subjects. In addition, the site of formation of critical tissue bubbles is unclear. Not only is there a lack of knowledge about where damaging bubbles are located in the body and where they arise (42), but there are also uncertainties inherent in our calculations. Several simplifications were made as follows. First, the tissue was assumed to be perfused by an infinite number of infinitesimally small capillaries (17, 18), and the tissue element was assumed to be well stirred. The overall O_2 pressure gradient in the macro- and microsystem [$\Phi_{O_2}(t)$] was considered homogeneous in the simulated large population of tissue elements/bubbles. Second, we assumed a resting value of $t_{1/2,N_2}$ of 360 min, which has been well documented for "standard" NASA and US Air Force altitude exposures (6–8). We then obtained a corresponding value of $t_{1/2,O_2}$ (313.2 min), through a derived relationship to $t_{1/2,N_2}$ (see *Eq. A13*). Third, blood flow in tissues and exercising skeletal muscles has not yet been measured during altitude. We therefore approximated $t_{1/2,N_2}$ and $t_{1/2,O_2}$ using a rough linear relationship between O_2 consumption and corresponding hypothetical blood flow (1, 25, 26) for an average subject performing mild, moderate, and heavy exercise. Furthermore, physical properties of the tissue such as the overall solubility are modified by exercise-induced tissue hyperemia. Therefore, *Eq. A13* should be modified with adjustments of blood flow with exercise along with the solubility of the tissue. However, we were unable to assess the change of tissue solubility with exercise. Fourth, we neglected the possible effects of the expected local temperature rise (1–2°C) in critical tissues during the simulated submaximal exercises. From the equation of state of an ideal gas, this minor change of ≤0.64% on the Kelvin scale would have negligible effect on the bubble volume. With this small temperature rise, physical constants such as solubilities and diffusivities of gases in tissues would also be expected to remain nearly constant (24). Fifth, even though the metabolic production of CO_2 may increase at the onset of our simulated submaximal aerobic exercise, we assumed that the dissolved CO_2 tissue tension (Pti_{CO_2}) remains approximately constant during the ensuing steady-state phase due to the concurrent decrease in arterial CO_2 tension (Pa_{CO_2}) (27). Sixth, the effects of gas diffusion and coalescence between bubbles within a unit of tissue volume were neglected. Seventh, an increase of intramuscular interstitial pressure during skeletal muscle contractions, which may affect the tissue elastic recoil (ν) and bubble growth, was not considered in our study.

Perspectives

Our simulations suggest that exercise-induced elevation of O_2 consumption at altitude leads to bubble persistence in tissues. At the same time, however, exercise-enhanced perfusion leads to an overall suppression of bubble growth. The total volume of bubbles would be reduced unless increased tissue motion simultaneously raises the rate of bubble formation (larger values of the Poisson process parameter β) through cavitation processes, thus maintaining or increasing total bubble volume, despite the exercise. Whether the rate of bubble formation and the incidence of DCI are associated with specific types of mechanical movement of body structures (19) remains to be investigated. Furthermore, measurements of cardiac output and local blood flows in skeletal muscles of a limb, presently under way, will provide further insight into the effects of exercise-induced circulatory changes, particularly during the O_2 prebreathe, on the incidence of altitude bubbles and DCI.

APPENDIX

The appendix introduces the intermediate steps necessary before calculation of $R_b(t)$ using *Eq. 6*. After a partial O_2 pressure change, mixing of inspired O_2-enriched mixtures with lung resident gas is assumed to be approximately complete within 1 min. $P_{A_{O_2}}$ and $P_{A_{N_2}}$ are estimated from the alveolar gas equations (11, 42).

Calculation of L(t) and L̇(t). Various homeostatic processes maintain $m_{CO_2}(t)$ and $m_{H_2O}(t)$ relatively constant; hence, these two terms can be neglected in the differentiation of $M_{ti}(t)$ and $M_b(t)$ in *Eq.* 5. When *Eqs. 2–5* are combined, the quantity

$$L(t) = \frac{1}{RT}\left[s_{ti,N_2} Pti_{N_2}(t) + s_{ti,O_2}\Phi_{O_2}(t)\right],\ t > t_b \qquad (A1)$$

and its time derivative $\dot{L}(t)$ occur explicitly in the expression for $R_b(t)$ given by *Eq. 6*. To obtain $\dot{L}(t)$, we used *Eqs. 7* and *9* to calculate

$$\dot{P}ti_{N_2}(t) = -k_1[Pti_{N_2}(t_b) - Pa_{N_2}(t)]e^{-k_1(t-t_b)} \qquad (A2)$$

$$\dot{\Phi}_{O_2}(t) = -k_2[\Phi_{O_2}(t_b) + \Psi_{O_2}(t) + (A - a)PO_2(t)]e^{-k_2(t-t_b)} \qquad (A3)$$

Calculation of K(t) and K̇(t). The expression

$$K(t) = \frac{1}{RT}\left[P_{b,N_2}(t) + P_{b,CO_2}(t) + P_{b,O_2}(t) + P_{b,H_2O}(t)\right],\ t > t_b \qquad (A4)$$

also occurs in the derivation of *Eq. 6*. Dissolved gases surrounding the bubble add to the surface tension pressure and

to the elastic recoil of the tissue, which resists expansion. With the use of the Laplace law (4, 13, 14) and application to all dissolved gases, $P_{b,N_2}(t)$, part of the expression of $K(t)$, may be expressed as follows

$$P_{b,N_2}(t) = \Phi_{O_2}(t) + Pti_{N_2}(t) + Pti_{CO_2}(t) + Pti_{H_2O}(t) + \varphi_1(t) - P_{b,mg}(t) \quad (A5)$$

In *Eq. A5*, $\varphi_1(t)$ is the sum of pressures due to surface tension and tissue elastic recoil. With the assumption of perfect spherical bubble, $\varphi_1(t)$ can be expressed in terms of the radius $R_b(t)$

$$\varphi_1(t) = \frac{2\tau}{R_b(t)} + \frac{4}{3}\pi R_b^3(t)\nu \quad (A6)$$

where τ is the surface tension at the bubble-tissue interface and ν is the tissue elastic recoil. The last term in *Eq. A5*, total pressure in the bubble due to metabolic gases, is expressed in terms of its components

$$P_{b,mg}(t) = P_{b,CO_2}(t) + P_{b,O_2}(t) + P_{b,H_2O}(t) \quad (A7)$$

By use of *Eqs. A5–A7,* it follows that

$$\dot{K}(t) = \frac{1}{RT}[\dot{\Phi}_{O_2}(t) + Pti_{H_2O} + \dot{\varphi}_1(t)] \quad (A8)$$

where $\varphi_1(t)$ is readily obtained from *Eq. A6*. Note that Pti_{CO_2} and Pti_{H_2O}, being constant, do not contribute to $\dot{K}(t)$.

Approximation of the O_2 pressure in the bubble. To obtain the net flux across the diffusion barrier with *Eq. 3*, we need $P_{b,O_2}(t)$. According to Fick's first law (33), the flux of O_2 passing through the surface of the boundary layer at *time t*, $\hat{J}_{O_2}$, is approximately given by

$$\hat{J}_{O_2}(t) = \frac{-D_{O_2}}{RT\epsilon}\{s_{ti,O_2}[-\Phi_{O_2}(t)] - P_{b,O_2}(t)\} \quad (A9)$$

From the law of conservation of mass (14, 33), we have

$$A_b(t)J_{O_2}(t) = \dot{M}_{ti,O_2}(t),\ t > t_b \quad (A10)$$

It has been shown that, for N_2, linear gas exchange kinetics in tissues are invoked for long half times for which the tension of dissolved gases exceeds ambient pressure (30, 31). With the assumption of similar kinetics for O_2, $M_{ti,O_2}(t)$ is approximately linear in t for $t > t_b$. Therefore, we readily obtain $\dot{M}_{ti,O_2}(t) \cong M_{ti,O_2}(t)/(t - t_b)$; $M_{ti,O_2}(t_b) = 0$. Also, according to Henry's Law, we can write

$$M_{ti,O_2}(t) = \frac{V_b(t)}{RT}[s_{ti,O_2}h\Phi(t) - P_{b,O_2}(t)] \quad (A11)$$

From *Eqs. A9–A11*, it follows that

$$P_{b,O_2}(t) = s_{ti,O_2}\Phi_{O_2}(t)\frac{hR_b(t)\epsilon(t) - 3D_{O_2}\Delta t}{R_b(t)\epsilon(t) + 3D_{O_2}\Delta t},\ \Delta t = t - t_b \quad (A12)$$

(Recall that $h = Vti/V_b$ is assumed constant.)

Relationship between O_2 and N_2 tissue half times. Let $\dot{Q}ti(t)$ be the blood flow in the homogeneous tissue with volume $Vti(t)$ at *time t*. Also let s_{b,N_2} and s_{ti,N_2} be the solubilities of N_2 in blood and tissue, respectively, and let s_{b,O_2} and s_{ti,O_2} be similar characteristics for O_2 (Table 2). The half times k_1 and k_2 for N_2 and O_2 (4, 14) are then given by

$$k_i = \frac{s_{b,i}\dot{Q}ti(t)}{s_{ti,i}Vti(t)} \quad (A13)$$

where $i = 1$ or 2. Therefore, given k_1, we may obtain $k_2 = \Omega k_1$ without knowledge of blood flow and tissue shell volume, where Ω is a constant [$t_{1/2,O_2} = (1/\Omega)t_{1/2,N_2}$ with $1/\Omega = 1/(0.0227/0.02) \times (0.0150/0.146) \approx 0.87$].

Generation of simulated bubble creation times. In terms of our application, Parzen's result can be stated as follows: "Given $N_i(T)$, the bubble creation times $t_{b,ij}$ are distributed as order statistics corresponding to $N_i(T)$ independent random variables with common cumulative distribution function $F(t) = m(t)/m(T)$ ($t_{alt} \le t \le T$)." In accordance with this result, we generated the unordered times $t'_{b,ij} = F^{-1}(U_{ij}) = -(1/\beta)\log[1 - U_{ij}(1 - e^{-\beta T})]$, where the U_{ij} were independent uniform (0,1) random variates [$j = 1,\ldots,N_i(T)$]. The $t'_{b,ij}$ were then sorted in ascending order to obtain the $t_{b,ij}$.

The authors acknowledge Drs. Bruce D. Butler, Joseph R. Rodarte, and Michael B. Reid for critically reading the manuscript. The authors thank Dr. Johnny Conkin for useful advice and Dr. Michael L. Gernhardt for the many discussions.

This study was supported by National Aeronautics and Space Administration Cooperative Agreement NCC9-58.

REFERENCES

1. **Armstrong RB, Delp MD, Goljan EF, and Laughlin MH.** Distribution of blood flow in muscles of miniature swine during exercise. *J Appl Physiol* 62: 1285–1298, 1987.
2. **Berghage TE, Wooley JM, and Keating LJ.** The probabilistic nature of decompression sickness. *Undersea Biomed Res* 1: 189–196, 1974.
3. **Burkard ME and Van Liew HD.** Effects of physical properties of the breathing gas on decompression bubbles. *J Appl Physiol* 79: 1828–1836, 1995.
4. **Burkard ME and Van Liew HD.** Simulation of exchanges of multiple gases in bubbles in the body. *Respir Physiol* 95: 131–145, 1994.
5. **Clark JM and Lambertsen CJ.** Alveolar-arterial O_2 differences in man at 0.2, 1.0, 2.0, and 3.5 Ata inspired P_{O_2}. *J Appl Physiol* 30: 753–763, 1971.
6. **Conkin J, Foster PP, Powell MR, and Waligora JM.** Relationship of the time course of venous gas bubbles to altitude decompression. *Undersea Biomed Res* 23: 141–149, 1996.
7. **Conkin J, Powell MR, Foster PP, and Waligora JM.** Information about venous gas emboli improves prediction of hypobaric decompression sickness. *Aviat Space Environ Med* 69: 8–16, 1998.
8. **Conkin J, Kumar KV, Powell MR, Foster PP, and Waligora JM.** A probabilistic model of hypobaric decompression sickness based on 66 chamber tests. *Aviat Space Environ Med* 67: 176–183, 1996.
9. **Di Prampero PE and Ferretti G.** Factors limiting maximal oxygen consumption in humans. *Respir Physiol* 80: 113–128, 1990.
10. **Ferretti G and Di Prampero PE.** Factors limiting maximal O_2 consumption: effects of acute changes in ventilation. *Respir Physiol* 99: 259–271, 1995.
11. **Foster PP, Conkin J, Powell MR, Waligora JM, and Chhikara RS.** Role of metabolic gases in bubble formation during hypobaric exposures. *J Appl Physiol* 83: 1088–1095, 1998.

11a. **Foster PP, Feiveson AH, and Boriek AM.** Predicting time to decompression illness during exercise at altitude, based on formation and growth of bubbles. *Am J Physiol Regulatory Integrative Comp Physiol* 279: R2317–R2328, 2000.

12. **Fukuba Y, Miura A, Kan A, Yanagawa K, and Sato H.** Functional diffusive/convective interaction determining maximal oxygen uptake in humans: its modeling perspective. *Appl Human Sci* 14: 259–270, 1995.
13. **Gault KA, Tikuisis P, and Nishi RY.** Calibration of a bubble evolution model to observed bubble incidence in divers. *Undersea Hyperb Med* 22: 249–262, 1995.
14. **Gernhardt ML.** *Development and Evaluation of a Decompression Stress Index Based on Tissue Bubble Dynamics* (Ph.D.

dissertation). Philadelphia, PA: University of Pennsylvania, 1991, p. 112–142.
15. **Gordon McDowall D, Ledingham IM, and Tindal S.** Alveolar-arterial gradients for oxygen at 1, 2, and 3 atmospheres absolute. *J Appl Physiol* 24: 324–329, 1968.
16. **Hills BA and LeMessurier DH.** Unsaturation in living tissue relative to the pressure and composition of inhaled gas and its significance in decompression theory. *Clin Sci* 36: 185–195, 1969.
17. **Hlastala MP.** Transient-state diffusion in rat subcutaneous tissue. *Aerospace Med* 45: 269–273, 1974.
18. **Hlastala MP and Van Liew HD.** Absorption of in vivo inert gas bubbles. *Respir Physiol* 24: 147–158, 1975.
19. **Jankowski LW, Nishi RY, Eaton DJ, and Griffin AP.** Exercise during decompression reduces the amount of venous gas emboli. *Undersea Hyperb Med* 24: 59–65, 1997.
20. **Jauchem JR.** Effects of exercise on the incidence of decompression sickness: a review of pertinent literature and current concepts. *Int Arch Occup Environ Health* 60: 313–319, 1988.
21. **Katz M.** New formulation of water and macromolecular flux which corrects for non-ideality: theory and derivation, predictions, and experimental results. *J Theor Biol* 112: 369–401, 1985.
22. **Kumar KV, Calkins DS, Waligora JM, Gilbert JH, and Powell MR.** Time to detection of circulating microbubbles as a risk factor for symptoms of altitude sickness. *Aviat Space Environ Med* 63: 961–964, 1992.
23. **Lambertsen CJ, Ewing JH, Kough RH, Gould R, and Stroud MW.** Oxygen toxicity. Arterial and internal jugular blood gas composition in man during inhalation of air, 100% O_2, and 2% CO_2 in O_2 at 3.5 atmospheres ambient pressure. *J Appl Physiol* 8: 255–263, 1955.
24. **Langø T, Mørland T, and Brubakk AO.** Diffusion coefficients and solubility coefficients for gases in biological fluids and tissues: a review. *Undersea Hyperb Med* 23: 247–272, 1996.
25. **Laughlin MH.** Skeletal muscle blood flow capacity: role of muscle pump in exercise hyperemia. *Am J Physiol Heart Circ Physiol* 253: H993–H1004, 1987.
26. **Laughlin MH and Armstrong RB.** Muscular blood flow distribution patterns as a function of running speed in rats. *Am J Physiol Heart Circ Physiol* 243: H296–H306, 1982.
27. **Lindinger MI, Spriet LL, Hultman E, Putman T, McKelvie RS, Lands LC, Jones NL, and Heigenhauser GJF.** Plasma volume and ion regulation during exercise after low- and high-carbohydrate diets. *Am J Physiol Regulatory Integrative Comp Physiol* 266: R1896–R1906, 1994.
28. **Muller I.** On diffusion and thermal diffusion in a mixture of Maxwellian gases. *Arch Rational Mech Anal* 31: 255–270, 1968.
29. **Olszowka AJ and Farhi LE.** A system of digital computer subroutines for blood gas calculations. *Respir Physiol* 4: 270–280, 1968.
30. **Parker E, Survanshi SS, Massell PB, and Weathersby PK.** Probabilistic models of the role of oxygen in human decompression sickness. *J Appl Physiol* 84: 1096–1102, 1998.
31. **Parker E, Survanshi SS, Weathersby PK, and Thalmann ED.** *Statistically Based Decompression Tables. VIII. Linear-Exponential Kinetics.* Bethesda, MD: Naval Medical Research Institute, 1992. (NMRI Rep. 92-73)
32. **Parzen E.** Counting processes and Poisson processes. In: *Stochastic Processes,* edited by Lehmann EL. San Francisco, CA: Holden-Day, 1967, p. 136–147.
33. **Rahn H, Paganelli C, and Ar A.** Pores and gas exchange of avian eggs: a review. *J Exp Zool Suppl* 1: 165–172, 1987.
34. **Reinertsen RE, Flook V, Koteng S, and Brubakk A.** Effects of oxygen tension and rate of pressure reduction during decompression on central gas bubbles. *J Appl Physiol* 84: 351–356, 1998.
35. **Severinghaus JW.** Blood gas calculator. *J Appl Physiol* 21: 1108–1116, 1966.
36. **Severinghaus JW.** Simple, accurate equations for human blood O_2 dissociation computations. *J Appl Physiol* 46: 599–602, 1979.
37. **Sylvester JT, Cymerman A, Gurtner G, Hottenstein O, Cote M, and Wolfe D.** Components of alveolar-arterial O_2 gradient during rest and exercise at sea level and high altitude. *J Appl Physiol* 50: 1129–1139, 1981.
38. **Taylor HM and Karlin S.** Poisson processes. In: *An Introduction to Stochastic Modeling*. San Diego, CA: Academic, 1994, p. 4–6, 27–30, 244–300.
39. **Tikuisis P, Gault KA, and Nishi RY.** Prediction of decompression illness using bubble models. *Undersea Hyperb Med* 21: 129–143, 1994.
40. **Van Liew HD and Burkard ME.** Density of decompression bubbles and competition for gas among bubbles, tissue, and blood. *J Appl Physiol* 75: 2293–2301, 1993.
41. **Van Liew HD and Burkard ME.** Simulation of gas bubbles in hypobaric decompressions: roles of O_2, CO_2, and H_2O. *Aviat Space Environ Med* 66: 50–55, 1995.
42. **Van Liew HD, Conkin J, and Burkard ME.** The oxygen window and decompression bubbles: estimates and significance. *Aviat Space Environ Med* 63: 859–865, 1993.
43. **Van Liew HD and Hlastala MP.** Influence of bubble size and blood perfusion on absorption of gas bubbles in tissues. *Respir Physiol* 7: 111–121, 1969.
44. **Vann RD.** Exercise and circulation in the formation and growth of bubbles. In: *Supersaturation and Bubble Formation in Fluids and Organisms*, edited by Brubbakk AO, Hemmingsen BB, and Sundnes G. Trondheim, Norway: Tapir, 1989, p. 235–264.
45. **Weathersby PK, Hart BL, Flynn ET, and Walker WF.** Role of oxygen in the production of human decompression sickness. *J Appl Physiol* 63: 2380–2387, 1987.
46. **Weathersby PK and Homer LD.** Solubility of inert gases in biological fluids and tissues: a review. *Undersea Biomed Res* 7: 277–296, 1980.
47. **Weathersby PK, Homer LD, and Flynn ET.** On the likelihood of decompression sickness. *J Appl Physiol* 57: 815–825, 1984.
48. **Webb JT, Fischer MD, Heaps CL, and Pilmanis AA.** Exercise-enhanced preoxygenation increases protection from decompression sickness. *Aviat Space Environ Med* 67: 618–624, 1996.
49. **Wolfram S.** *MATHEMATICA: A System for Doing Mathematics by Computer.* Champaign, IL: Wolfram Research, 1996, version 3.01.
50. **Yount DE.** On the evolution, generation, and regeneration of gas cavitation nuclei. *J Acoust Soc Am* 71: 1473–1481, 1982.